Supplement of "Enhanced Moisture Delivery into Victoria Land, East Antarctica During the Early Last Interglacial: Implications for West Antarctic Ice Sheet Stability"

Yuzhen Yan[1,2], Nicole E. Spaulding[3], Michael L. Bender[1,4], Edward J. Brook[5], John A. Higgins[1], Andrei V. Kurbatov[3], Paul A. Mayewski[3]

[1]Department of Geosciences, Princeton University, Princeton NJ 08544, USA
[2]Department of Earth, Environmental and Planetary Sciences, Rice University, Houston TX 77005, USA
[3]Climate Change Institute, University of Maine, Orono ME 04469, USA
[4]School of Oceanography, Shanghai Jiao Tong University, Shanghai 200240, China
[5]College of Earth, Ocean, and Atmospheric Sciences, Oregon State University, Corvallis OR 97331, USA

***Correspondence to*: Yuzhen Yan (yuzhen.yan@rice.edu)**

Supplementary Text

Supplementary Figure (S1-S8)

Supplementary Data Table (1-4; uploaded as separate files)

Here, we describe how the uncertainties associated with the S27 gas chronology, the ice chronology, and Δage are estimated.

1 S27 gas age uncertainties

Recall Equation (4) in the main text, in which we built the following function:

$$\zeta(t) = \delta^{18}O_{atm(t),\,S27} - \delta^{18}O_{atm(t),\,EDC} \quad \text{(S1)}$$

Note the $\delta^{18}O_{atm(t),\,EDC}$ is linearly interpolated between discrete analyses. The benefit of expressing synchronization in the form of Equation (S1), instead of simply asking at what time (t) $\delta^{18}O_{atm(t),\,S27} = \delta^{18}O_{atm(t),\,EDC}$, is that uncertainties can be rigorously defined and quantitatively calculated. The final chronology uncertainty has three components as discussed separately below.

1.1 Analytical uncertainties associated with $\delta^{18}O_{atm}$

S27 and EDC $\delta^{18}O_{atm}$ are independent variables. As a result, the uncertainty of $\zeta(t)$ is given by:

$$\sigma_\zeta = \sqrt{\sigma_{S27}^2 + \sigma_{EDC}^2} \quad \text{(S2)}$$

where σ_{EDC} is the pooled standard deviation of the EDC $\delta^{18}O_{atm}$ data (0.028 ‰; Extier et al, 2018) and σ_{S27} is 0.046 ‰. Taking 0.028 ‰ and 0.046 ‰ into Equation (S2), the integrated uncertainty (1σ) for $\zeta(t)$ is 0.054 ‰. Because each depth has two duplicates, the width of 95 % confidence interval (CI) of $\zeta(t)$ is ±0.076 ‰ (calculated as 0.054 ‰ multiplied by 2, and then divided by the square root of 2) assuming a Gaussian distribution.

1.2 Age uncertainties relative to the EDC chronology

In order to translate the integrated analytical uncertainties (±0.076 ‰) into age uncertainties, we repeat the direct matching process described in the main text. This time, however, we attempt to link the highest and lowest value of the 95 % CI of each S27 $\delta^{18}O_{atm}$ datum (that is, $\delta^{18}O_{atm(t),\,S27} \pm 0.076$ ‰) to the $\delta^{18}O_{atm(t),\,EDC}$ series. 28 out of the 51 samples whose age was assigned by direct matching have their age uncertainties determined this way (marked as "95 % CI directly matched" in Supplementary Data Table 3). The age uncertainties of the remaining 55 points were interpolated from the nearby age points that were successfully assigned age uncertainties via direct matching (Figure 3). Here, ice stratigraphy puts an implicit constraint on how age uncertainties could vary with depth.

1.3 Uncertainties in EDC chronology

The chronology of EDC reported by Extier et al (2018) is AICC2012, the most up-to-date and internally consistent chronology derived from multiple Antarctic ice cores (Veres et al, 2013; Bazin et al, 2013). AICC2012 has its own dating uncertainties, which are independent from the uncertainties arising from the $\delta^{18}O_{atm}$ analyses. We thus combined these two types of

uncertainties quadratically, similar to Equation (S2), and separately calculated the lower and upper bound of the 95 % confidence interval for the final absolute gas chronology.

2 S27 ice age uncertainties

Since no uncertainty estimate is available for the ice chronology established in Spaulding et al (2013), we calculate the uncertainties associated with δD_{ice} synchronization here. Similar to the case of gas chronology, the absolute uncertainty of the ice chronology consists of (1) the analytical errors in δD_{ice}, (2) age errors in S27 ice chronology relative to the EDC ice chronology, and (3) the intrinsic uncertainties of the EDC ice chronology itself.

Because S27 δD_{ice} was measured in large numbers with high analytical precision (±0.05 ‰; Spaulding et al, 2013), we expect minimal analytical errors for the ice chronology. Next, we consider the uncertainty of S27 ice chronology relative to the EDC age scale, which depends on two factors: the synchroneity of temperature variations across Antarctica and how precisely peaks in two time series can be identified and tied.

The assumed synchroneity between S27 and Taylor Dome is supported by their physical proximity (115 km). Modelling results in addition show that in the event of a collapsed WAIS, both the EDC and Taylor Dome sites are going to experience the same trend in temperature changes (Steig et al., 2015). In addition, the overall deglacial warming is almost synchronous during Termination I in the Taylor Dome (closest deep core to S27) and EDC (the matching target of S27 δD_{ice}) stable water isotope records (Stenni et al., 2011). Both records have an apparent mismatch in peak $\delta^{18}O_{ice}$ around 14 ka, right before the Antarctic Cold Reversal. This offset is about 200 years, translating to the uncertainty of ±100 years associated with the aligning EDC and Taylor Dome ice cores, and by inference, between EDC and S27. Beyond 15 ka, the resolution of Taylor Dome isotope record becomes too low to permit an effective comparison.

Second, because the ice age tie-points are based on the maximum or minimum isotope peaks, and the peaks in the record were based on discrete sample analysis, the real peak in the record might not be sampled and captured in the observation. Intuitively, the higher the sampling resolution, the smaller the chance of missing the real peak. In the worst-case scenario, the real peak could be located infinitely close to the two samples next to the observed peak. If the sampling resolution is 100 years, for example, then the maximum error associated with identifying the peak in this record is 200 years. In the case of EDC and S27, the average sampling resolution of stable water isotopes during MIS 5e is ~40 and ~20 years, respectively. In attempting to tie the peaks, their respective errors should be added up. In the case of EDC and S27, therefore, the identification and matching peaks in different isotope records has an uncertainty of ±60 years.

Taking these two sources of uncertainties together, the ice age tie-points have a nominal uncertainty of ±160 years. For the sake of simplicity, we treat this value as the two standard deviations (2σ), though we note that the true probability function distribution is not clear. This number should be viewed as a conservative estimate of the ice age uncertainties, as there could

be multiple δD_{ice} peaks in the S27 ice core that might correspond to a stable water isotope peak in EDC. As a result, the true uncertainty of the ice age scale might be larger. Here we evaluate how the ambiguity of δD_{ice} tie-points could potentially impact the Δage and accumulation rate estimates, especially since the minimum Δage around 128 ka is predicated upon the δD_{ice} tie-point at 128.33 ka (Figure S7). For example, we cannot rule out the possibility that it is the δD_{ice} peak at 128.01 ka in the original Spaulding et al (2013) ice chronology that corresponds to the EDC peak at 128.33 ka, meaning that the original tie-point was misaligned by 300 years. If that is the case and we retain the δD_{ice} tie-point at 126.05 and 135.81 ka, the new minimal Δage will be 759 yr (Figure S8). By contrast, the minimal Δage inferred from the original ice chronology is 145 yr. Under this alternative tie-point scenario, the estimated highest accumulation rate is 0.019 m yr^{-1} (95 % CI: 0.011~0.046 m yr^{-1}). Furthermore, in order for Δage to remain persistently higher than ~2000 yrs during the LIG (Figure S8), the 128.33 ka EDC δD_{ice} needs to be tied to the S27 δD_{ice} peak at 127.25 ka in the original ice chronology (Figure S7). In other words, the S27 stable water isotope tie-point that is matched to the 128.33 ka EDC δD_{ice} peak has to be misaligned for ~1000 years.

Finally, the overall uncertainty of the S27 ice chronology is calculated by quadratically combining the uncertainty associated with isotope tie-points and the uncertainties of the EDC ice chronology (AICC2012).

3 Δage uncertainties

Now that gas and ice chronologies are independently constructed, we evaluate the uncertainties for the Δage, which affect accumulation rate estimates. Here, the absolute ice and gas age uncertainties cannot be simply combined quadratically, because the gas age and ice age are not independent. For example, the AICC2012 gas age scale is constructed on the basis of a model-based ice scale and lock-in depth (LID) estimate, unless the gas age is synchronized via stratigraphic links (Veres et al, 2013; Bazin et al, 2013).

The uncertainty associated with S27 Δage has three components: the relative uncertainty of S27 gas age to EDC gas age, the relative uncertainty of S27 ice age to EDC ice age, and the intrinsic uncertainty of EDC Δage (which is associated with the lock-in depth). The first two terms have been discussed above, and we discuss the intrinsic Δage uncertainties of the EDC chronology below.

The Δage uncertainty of EDC ice core in the AICC2012 timescale is not reported explicitly (Bazin et al, 2013). We use the relative errors of LID in EDC ice cores computed by the IceChrono model to infer the Δage uncertainties (Parrenin et al, 2015). Specifically, we calculated at each time the relative error of LID, as the ratio of standard deviation of LID to the LID. Between 110 and 145 ka, the relative error of EDC LID ranges from 12% to 48%, with interglacial periods associated with smaller errors. We then calculated the intrinsic Δage uncertainty associated with AICC2012 by multiplying this ratio with the S27 Δage values at the same age. This way we transferred the uncertainty embedded in the EDC LID estimates to S27 Δage uncertainty.

Combining these three sources of uncertainties quadratically similar to Equation (S2) yields the final uncertainty, presented in Supplementary Data Table 4. Prior to 130 ka, the intrinsic AICC2012 Δage uncertainties dominate the S27 Δage uncertainties. After 130 ka, the primary source of errors becomes the relative errors of S27 gas chronology to AICC2012 gas chronology. These Δage uncertainties are further propagated into the errors of accumulation rate estimates by Monte-Carlo simulation (Figure S5).

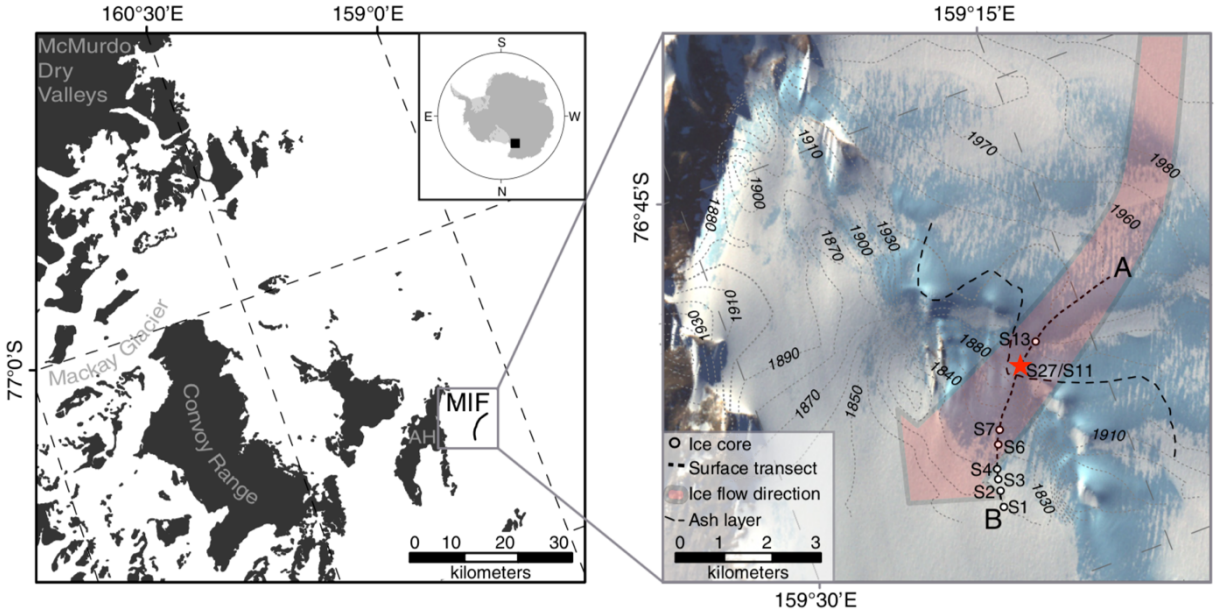

Figure S1: Geographic settings of the Allan Hills area (left) and the location of S27 ice cores (red star), modified after Spaulding et al (2013). Also shown on the right panel are a series of surface ice samples collected on the transect marked by the dashed line between A and B as well as shallow ice cores from S1 to S27. The red arrow shows the measured ice flow according to Spaulding et al (2012). Thin dashed lines mark the local elevation. The ash layer intercepting the transect A-B at S27 is one of the many ash layers used as an age reference point. Copyright © University of Washington.

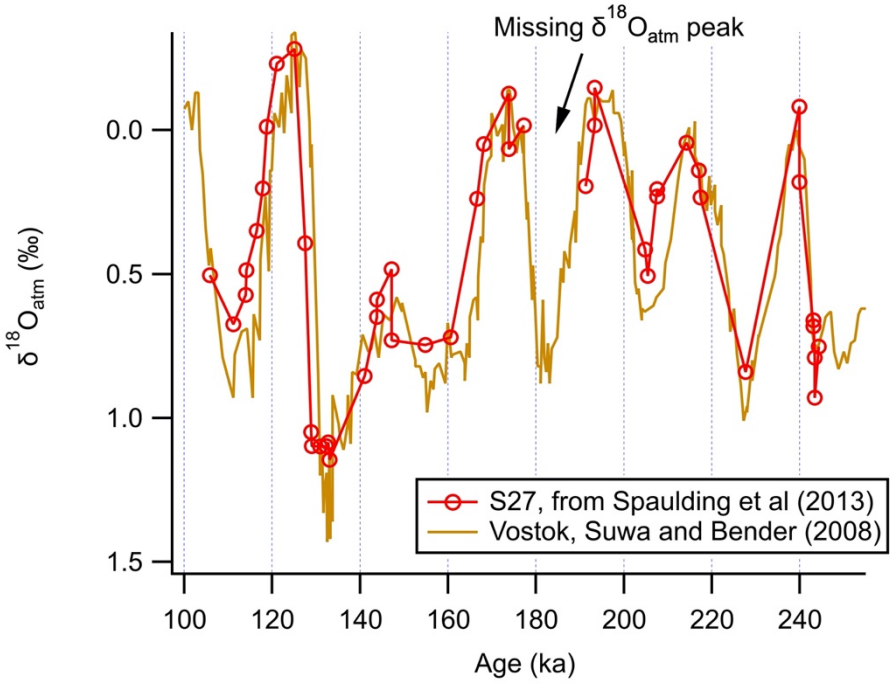

Figure S2: $\delta^{18}O$ of atmospheric O_2 ($\delta^{18}O_{atm}$) measurements from S27 (red) reported in Spaulding et al (2013) in comparison with the same property measured in Vostok (brown) by Suwa and Bender (2008). The location of the missing $\delta^{18}O_{atm}$ peak from ~180 ka from earlier measurements is indicated by the black arrow.

Depth <148 m:

2013: $\delta O_2/N_2$ (‰) = -0.0317*depth (m) - 8.79; 2018: $\delta O_2/N_2$ (‰) = -0.0360*depth (m) - 10.95

Depth >148 m:

2013: $\delta O_2/N_2$ (‰) = -0.205*depth (m) + 24.26; 2018: $\delta O_2/N_2$ (‰) = -0.106*depth (m) - 0.37

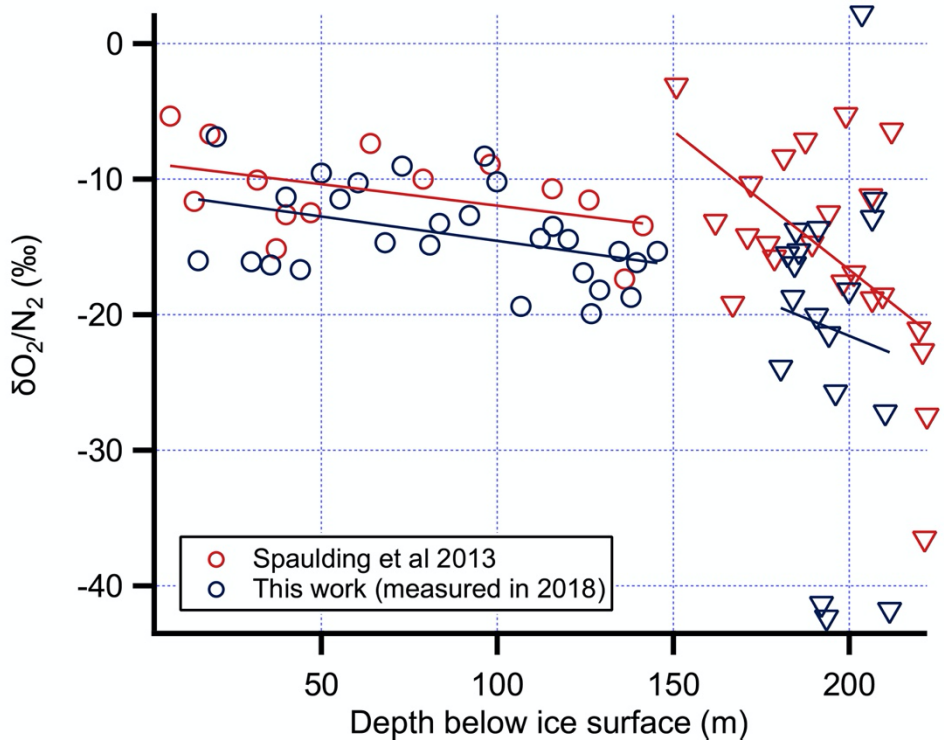

Figure S3: Depletion of $\delta O_2/N_2$ due to gas loss after five years in S27. $\delta O_2/N_2$ data points shown in red are from data measured in 2013, and $\delta O_2/N_2$ in dark blue were measured in 2018. Circles indicate $\delta O_2/N_2$ measurements on ice without any visible fracture, whereas triangles represent $\delta O_2/N_2$ measured on heavily fractured ice. The preferential loss of O_2 relative to N_2 is revealed by the lowered trend line (where $\delta O_2/N_2$ is regressed against depth). This offset in $\delta O_2/N_2$ is assumed to be depth-dependent and subsequently used in the gas loss correction. Note that new and earlier gas measurements were not carried on the exact same depth. The break in the lines at 148 m depth is arbitrary. It is the average depth of the deepest sample with good core quality (no fracture) and the shallowest fractured sample. The data could be represented by unbroken lines as well. However, given that the slope of $\Delta\delta^{18}O_{grav}$ vs. $\Delta\delta O_2/N_2$ is only 0.0067 ‰ ‰$^{-1}$ (Figure S4), the choice of regression lines here will have only a small impact on the subsequent data and analysis.

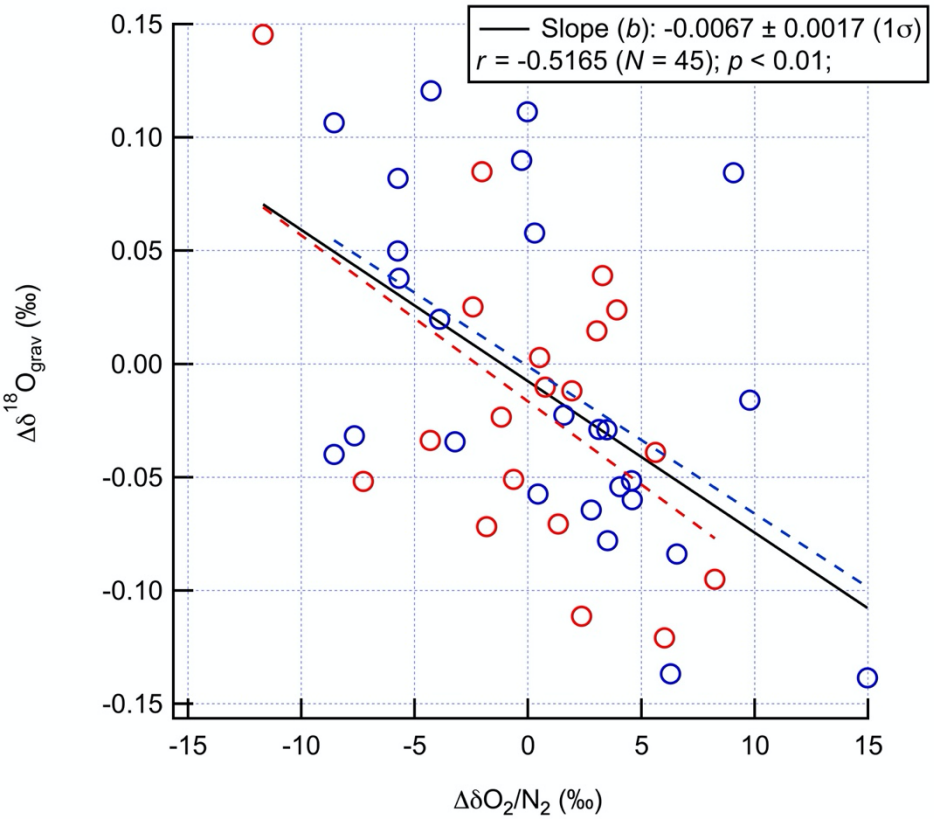

Figure S4: Impact on $\delta^{18}O_{atm}$ due to gas loss in S27 in ice without (blue) and with (red) visible fractures. The difference in the elemental and isotopic compositions between two replicates is attributable to gas loss. The slope of the regression line, *b*, of replicate $\delta^{18}O_{grav}$ differences on replicate $\delta O_2/N_2$ differences is used to correct for gas losses according to Equation (3) in the main text. There is no statistically significant difference between the regression slopes for fractured and non-fractured ice (dashed lines), so we combine the data and perform a unified gas loss correction (solid line). The magnitude of final gas loss correction is typically ~0.020 ‰.

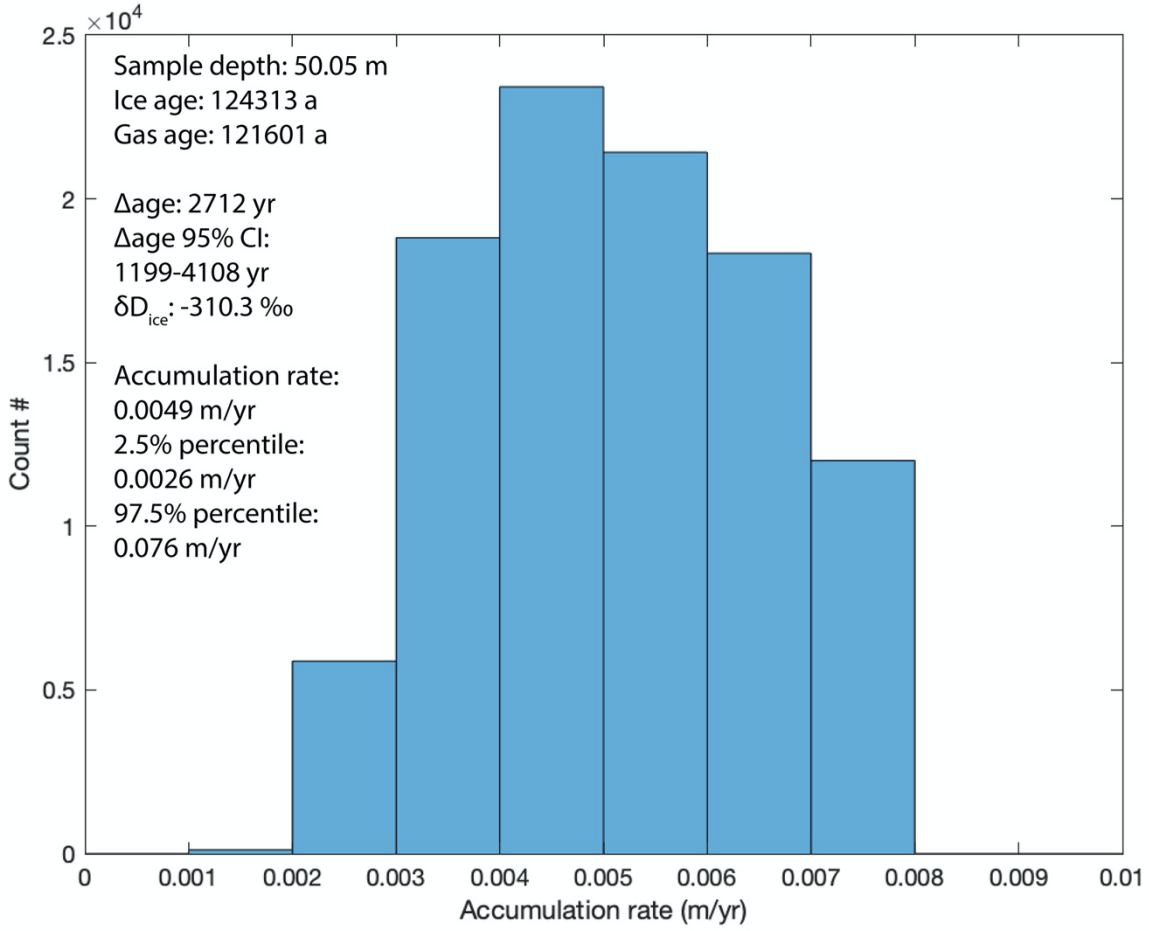

Figure S5: An example of the Monte Carlo simulation used to estimate the distribution of accumulation rates given known Δage and δD_{ice} values. The spread originates from the uncertainties in Δage. For each Δage datum, simulations are run 100,000 times to compute the probability distribution of accumulation rates. The mode of the 100,000 runs is reported as the accumulation rate corresponding to that Δage. Note that because the data is not normally distributed, taking the arithmetic average of the 100,000 estimated values would lead to apparent overestimation. To quantify uncertainties associated with the accumulation rate estimate, 2.5% and 97.5 % percentile values are taken as the lower and upper limits of the 95% confidence interval (CI), respectively. The final reported accumulation rate for this datum with a Δage of 2712 yr (95% CI: 1199-4108 yr) at 124.3 ka is 0.005 m yr^{-1} (95% CI: 0.003-0.076 m yr^{-1}).

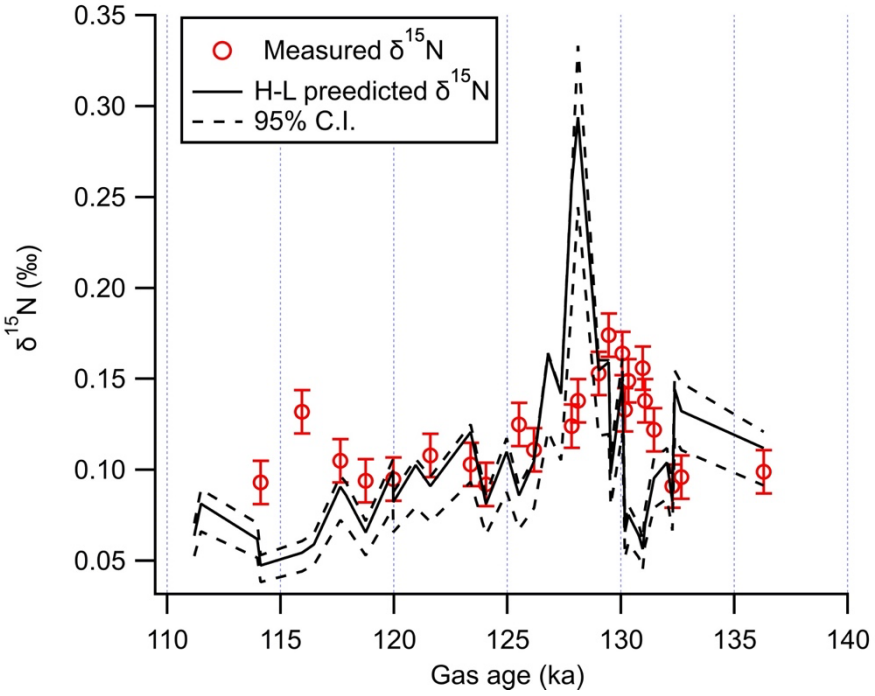

Figure S6: $\delta^{15}N$ values estimated from the H-L model (black) and measured in S27 ice (red). Dashed lines represent the 95% confidence interval (C.I.) of the model-predicted $\delta^{15}N$. Error bar associated with measured $\delta^{15}N$ values represent pool standard deviation of $\delta^{15}N$ measurements (0.012 ‰). When using the H-L model to predict $\delta^{15}N$, we assumed the height of the lock-in zone to be 3 m, and the height of convective zone to be 0 m.

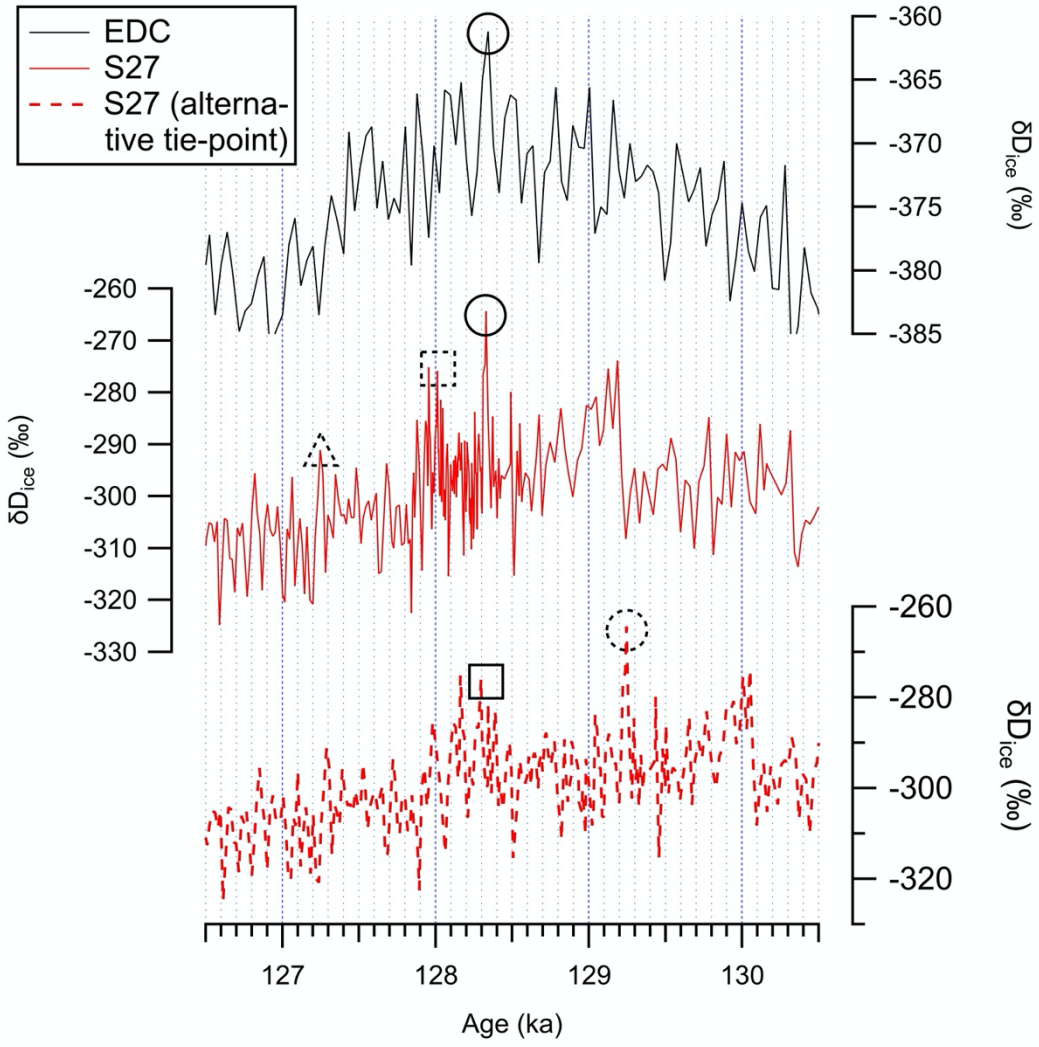

Figure S7. Evaluating alternative δD_{ice} tie-points around 128 ka and its impact on ice chronology. The top and middle panel are a zoom-in view of Figure 2 in the main text, with tie-points circled by solid lines. The lower panel shows the same δD_{ice} record under a different tie-point scheme: the δD_{ice} peak at 128.01 ka in the middle panel (dashed square) is tied to the EDC δD_{ice} peak at 128.33 ka. This new tie-point (square) leads to an older ice age at the same depth and hence larger Δage and smaller accumulation rates. In order for Δage to remain unchanged across the MIS 5e (Figure S8), the δD_{ice} peak around 127.25 ka (dashed triangle) needs to be tied to the 128.33 ka EDC δD_{ice} peak.

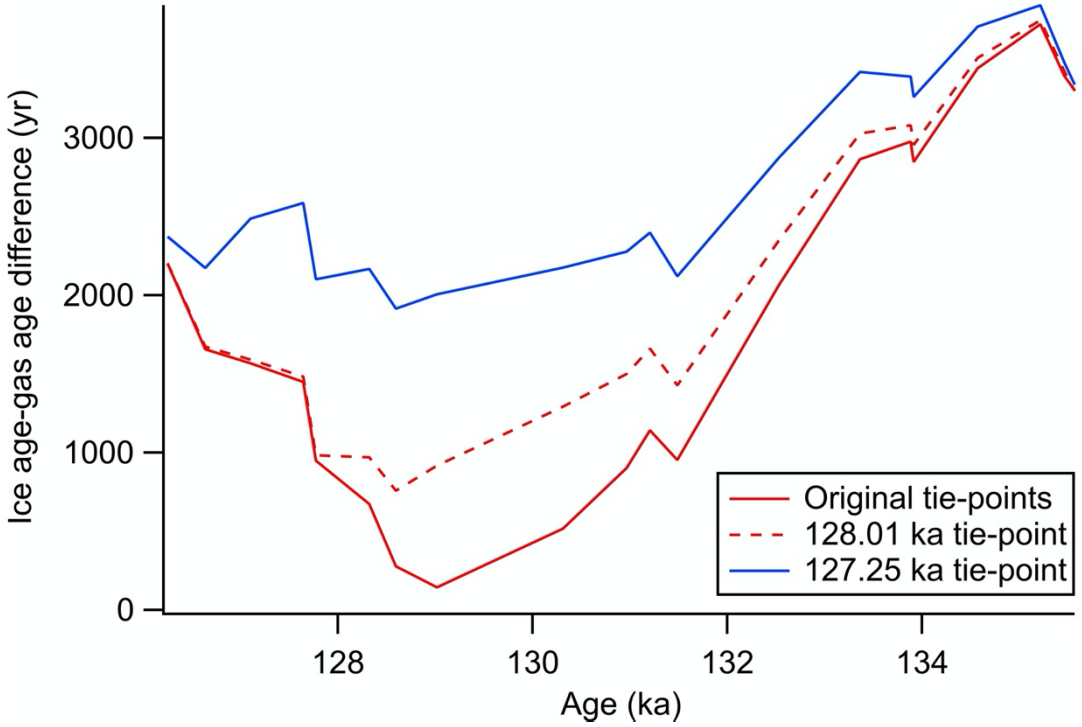

155

Figure S8. Δage estiamtes under different tie-point scenarios. Solid red: original tie-points adopted by Spaulding et al (2013) and used in this study (same as Figure 7 in the main text). Dashed red: S27 δD_{ice} at 128.01 ka tied to the EDC δD_{ice} at 128.33 ka (square in Figure S7). Solid blue: S27 δD_{ice} at 127.25 ka tied to the EDC δD_{ice} at 128.33 ka (triangle in Figure S7).

References

Bazin, L., Landais, A., Lemieux-Dudon, B., Kele, H.T.M., Veres, D., Parrenin, F., Martinerie, P., Ritz, C., Capron, E., Lipenkov, V. and Loutre, M.F.: An optimized multi-proxy, multi-site Antarctic ice and gas orbital chronology (AICC2012): 120-800 ka, Clim. Past, 9, 1715-1731, https://doi.org/10.5194/cp-9-1715-2013, 2013.

Extier, T., Landais, A., Bréant, C., Prié, F., Bazin, L., Dreyfus, G., Roche, D.M. and Leuenberger, M.: On the use of $\delta^{18}O_{atm}$ for ice core dating, Quaternary Sci. Rev., 185, 244-257, https://doi.org/10.1016/j.quascirev.2018.02.008, 2018.

Parrenin, F., Bazin, L., Capron, E., Landais, A., Lemieux-Dudon, B. and Masson-Delmotte, V.: IceChrono1: a probabilistic model to compute a common and optimal chronology for several ice cores, Geosci. Model Dev., 8, 1473-1492, https://doi.org/10.5194/gmd-8-1473-2015, 2015.

Spaulding, N.E., Higgins, J.A., Kurbatov, A.V., Bender, M.L., Arcone, S.A., Campbell, S., Dunbar, N.W., Chimiak, L.M., Introne, D.S. and Mayewski, P.A.: Climate archives from 90 to 250 ka in horizontal and vertical ice cores from the Allan Hills Blue Ice Area, Antarctica, Quaternary Res., 80, 562-574, https://doi.org/10.1016/j.yqres.2013.07.004, 2013.

Spaulding, N.E., Spikes, V.B., Hamilton, G.S., Mayewski, P.A., Dunbar, N.W., Harvey, R.P., Schutt, J. and Kurbatov, A.V.: Ice motion and mass balance at the Allan Hills blue-ice area, Antarctica, with implications for paleoclimate reconstructions, J. Glaciol., 58, 399-406, https://doi.org/10.3189/2012JoG11J176, 2012.

Steig, E.J., Huybers, K., Singh, H.A., Steiger, N.J., Ding, Q., Frierson, D.M., Popp, T. and White, J.W.: Influence of West Antarctic ice sheet collapse on Antarctic surface climate, Geophys. Res. Lett., 42, 4862-4868, https://doi.org/10.1002/2015GL063861, 2015.

Stenni, B., Buiron, D., Frezzotti, M., Albani, S., Barbante, C., Bard, E., Barnola, J.M., Baroni, M., Baumgartner, M., Bonazza, M. and Capron, E.: Expression of the bipolar see-saw in Antarctic climate records during the last deglaciation, Nat. Geosci., 4, 46-49, https://doi.org/10.1038/ngeo1026, 2011.

Suwa, M. and Bender, M.L.: Chronology of the Vostok ice core constrained by O_2/N_2 ratios of occluded air, and its implication for the Vostok climate records, Quaternary Sci. Rev., 27, 1093-1106, https://doi.org/10.1016/j.quascirev.2008.02.017, 2008.

Veres, D., Bazin, L., Landais, A., Toyé Mahamadou Kele, H., Lemieux-Dudon, B., Parrenin, F., Martinerie, P., Blayo, E., Blunier, T., Capron, E. and Chappellaz, J.: The Antarctic ice core chronology (AICC2012): an optimized multi-parameter and multi-site dating approach for the last 120 thousand years, Clim. Past, 9, 1733-1748, https://doi.org/10.5194/cp-9-1733-2013, 2013.